THE JOURNAL OF PHYSICAL CHEMISTRY C

Article

pubs.acs.org/JPCC

Interaction of Iron−Sulfur Clusters with N_2: Biomimetic Systems in the Gas Phase

Heiko C. Heim,[†] Thorsten M. Bernhardt,[†] Sandra M. Lang,[*,†,§] Robert N. Barnett,[‡] and Uzi Landman[*,‡]

[†]Institute of Surface Chemistry and Catalysis, University of Ulm, Albert-Einstein-Allee 47, 89069 Ulm, Germany

[§]Institute of Chemical Engineering, University of Ulm, Albert-Einstein-Allee 11, 89081 Ulm, Germany

[‡]School of Physics, Georgia Institute of Technology, Atlanta, Georgia 30332-0430, United States

Supporting Information

ABSTRACT: The active centers of the nitrogen-fixing enzymes nitrogenases comprise iron−sulfur clusters. The binding of the substrate N_2 to these clusters plays a fundamental role for the subsequent ammonia synthesis. However, due to the complexity of the natural system and the lack of suitable synthetic models, the interaction of N_2 with the iron−sulfur clusters remains largely elusive. In this contribution, we demonstrate the gas-phase preparation and investigation of the cationic $Fe_2S_2^+$, $Fe_3S_3^+$, and $Fe_4S_4^+$ clusters. These clusters represent the first cluster model systems containing more than one iron and sulfur atom, respectively, which are found to bind N_2. Temperature-dependent kinetic measurements allow, for the first time, for the determination of experimental binding energies of N_2 to iron−sulfur clusters. In addition, concurrent first-principles simulations reveal the ground state and isomeric structures of the iron−sulfur clusters with and without adsorbed N_2 and provide a conceptual understanding of the interaction between N_2 and iron−sulfur clusters. In particular, we present molecular level details of N_2 bonding such as the identification of the adsorption sites, the bond geometry, the bond strength, and the nature of the cluster-N_2 binding interaction, which is found to be promoted by occupation of the empty antibonding orbitals of the free N_2 molecule through interaction with the frontier orbitals of the iron−sulfur complex involving d-orbitals of iron hybridized with sulfur p-orbitals.

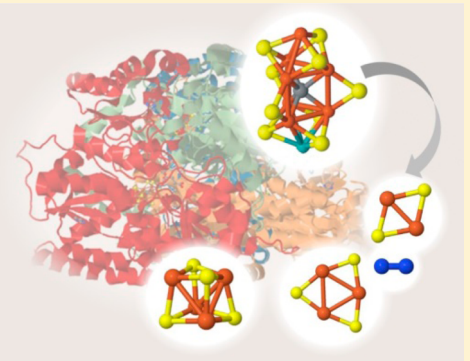

1. INTRODUCTION

Nitrogen represents an essential element for all living organisms. However, although N_2 is the most abundant molecule in the earth's atmosphere, it cannot be directly utilized but must be fixed, i.e., converted to more viable nitrogen-containing molecules such as ammonia or nitrate. Industrially, ammonia is synthesized in the Haber−Bosch process via the reaction of N_2 with H_2 mediated by an iron-based catalyst. However, the requirement of high temperatures and high pressures makes the Haber−Bosch synthesis an extremely energy-consuming process.[1,2]

In nature, N_2 is fixed at ambient pressure and temperature by the enzymes nitrogenases. So far, three different types of nitrogenases have unambiguously been identified: the FeMo-, FeV-, and Fe-only nitrogenase. All these nitrogenases are structurally very similar and comprise a series of different iron−sulfur clusters, which serve as electron-transport media as well as the FeM cofactor (M = Mo, V, Fe for FeMo-, FeV-, and Fe-only nitrogenases, respectively), which accepts electrons and protons and binds and catalytically converts the substrate N_2.[3−5]

High-resolution X-ray crystallography identified the core of the FeMo cofactor as a metal−sulfur cluster of the stoichiometry [Mo−7Fe−9S−C] (similar clusters [V−7Fe−9S−X] and [Fe−7Fe−9S−X] (X = a light atom), are assumed for FeV and FeFe cofactors)[6−12] and thus provided detailed structural understanding of the catalytically active center. Furthermore, considerable progress in the elucidation of the biological nitrogen fixation pathway has been made in recent years.[13−15] Despite these achievements, several aspects of the nitrogen reduction mechanism are still under discussion. One of the major open questions is, for example, related to the binding of the substrate, i.e., the exact binding site, the coordination of the N_2 molecule, and the nature of the interaction. Indeed, the interaction of the metal−sulfur cluster with N_2 represents one of the crucial reaction steps in the ammonia synthesis and is extremely important for understanding the mechanistic details of the subsequent N_2 reduction reaction.[16,17] The reasons for the limited understanding of N_2 binding are, on the one hand, the complexity of the FeMo cofactor and, on the other hand, the fact that the MoFe cofactor binds N_2 only after reduction of the FeMo cofactor with four electrons yielding the E_4H_4 state.[16−19] Thus, it is difficult to selectively populate this state for spectroscopic characterization.[14] So far, only Hoffman and co-workers have successfully trapped an intermediate during the early state of

Received: March 18, 2016
Revised: May 4, 2016

ACS Publications © XXXX American Chemical Society

DOI: 10.1021/acs.jpcc.6b02821
J. Phys. Chem. C XXXX, XXX, XXX−XXX

nitrogen reduction.[20,21] Spectroscopic studies of this intermediate indicated the end-on binding of N_2 to a metal atom.

With the aim of gaining a fundamental understanding of the nitrogen binding and the subsequent ammonia synthesis mechanism, numerous model complexes have been synthesized during the last decades. Surprisingly, simple metal atom complexes have been found to bind N_2 and have provided important insight into the catalytic reaction mechanism for N_2 reduction.[22−25] However, more structurally relevant models comprising multiple metal atoms and a sulfur environment appeared to lose the ability to bind N_2, which of course represents one of the foundations of functional relevance.[22,26] Only very recently has a novel model complex been synthesized that is able to bind N_2. This model includes iron−sulfur carbon sites and thus successfully accounts for the sulfur environment of iron in nitrogenase; however, it contains only one iron center and does not consider the presence of multiple metal atoms.[27] Thus, at this time, understanding of N_2 binding to the active center of nitrogenase is mainly based on theoretical simulations of model complexes, which are, however, limited by the enormous complexity of the FeMo cofactor.

Free iron−sulfur clusters represent a different class of model systems for the investigation of nitrogen binding and subsequent catalyzed reactions. However, previous gas-phase studies found cationic iron−sulfur clusters to be nonreactive toward N_2 under single collision conditions and after short reaction times, respectively.[28,29] In this paper, we present a new and unique approach by combining temperature-dependent kinetic experiments in an ion trap with first-principle simulations to enable for the first time a fundamental understanding of the substrate binding. We show that small iron−sulfur clusters $Fe_2S_2^+$, $Fe_3S_3^+$, and $Fe_4S_4^+$ are able to bind multiple N_2 under multicollision conditions in the ion trap and thus can be regarded as the first biomimetic systems, comprising several iron and sulfur atoms, respectively, which bind N_2. In particular, we show that N_2 prefers to bind to one of the iron atoms in an end-on configuration, and consequently, the binding geometry as well as the electronic interaction are found to be largely independent of cluster size.

2. METHODS

2.1. Experimental Setup. The experimental setup to study the reactivity of the iron−sulfur clusters consists of a variable-temperature radiofrequency (rf)−octopole ion trap inserted into a low energy ion beam assembly. The iron−sulfur cluster cations are produced by sputtering pyrite stone targets[30] with high energetic Xe ions which are generated in a cold reflex discharge ion source (CORDIS).[31] The cluster ion beam is steered into a helium-filled quadrupole ion guide to collimate and thermalize the hot clusters before mass selection of the cluster size of interest in a first quadrupole mass filter. The mass-selected clusters are then transferred via a second quadrupole ion guide into the home-built octopole ion trap,[32,33] which is prefilled with about 1 Pa of helium buffer gas as well as about 0.1 Pa of N_2. The ion trap is attached to a closed cycle helium cryostat that allows for temperature adjustment in the range between 20 and 300 K. Thermal equilibration of the clusters is achieved within a few milliseconds under these pressure conditions, while the clusters are stored for a considerably longer time, typically between 0.1 and 2 s.[32]

After a chosen reaction time, all ionic reactants, intermediates, and final products are extracted from the ion trap and mass-analyzed by a second quadrupole mass filter. By recording all ion intensities as a function of the reaction time, the kinetics at a well-defined reaction temperature can be obtained.

2.2. Theoretical Methods. The theoretical explorations of the atomic arrangements and electronic structures of the iron−sulfur clusters and their complexes with dinitrogen were performed with the use of the Born−Oppenheimer spin density-functional theory molecular dynamics (BO-SDFT-MD) method[34] with norm-conserving soft (scalar relativistic for Fe) pseudopotentials[35] and the generalized gradient approximation (GGA)[36] for electronic exchange and correlations. The BO-SDFT-MD method[34] is particularly suitable for investigations of charged systems since it does not employ a supercell (i.e., no periodic replication of the ionic system is used).

In all of the calculations, the dependence on spin multiplicity has been checked, and the results that we report correspond to the spin multiplicities with the lowest energies (global minimum for the ground-state configuration and local minimum for the isomeric structures); both spin and geometrical isomers are explored. The cluster is initially set up using atomic wave functions, with each iron atom having either five up-spin 3d orbitals fully occupied and five down-spin orbitals with an occupancy of 0.2 each or vice versa. All possible combinations were attempted, including geometry optimization with the orbital occupancy determined by the Fermi distribution function. Evaluation of the energy of the cationic clusters started with removal of an electron from the highest occupied orbital followed by optimization of the cluster geometry and occupancy. We have also tested some cases in which the Fe atoms were not initialized with fully occupied majority spin 3d orbitals, but these failed to yield a lower final energy. In the following, we denote the difference between the number of majority and minority spin electrons (spin-up and spin-down electrons) by $\mu = N_\uparrow - N_\downarrow$; spin-related quantities are expressed as 0.5μ. For analysis of the spatial distribution of majority and minority spins and clusters' antiferromagnetic arrangements, see our discussion below in connection with Figure 4.

The energy minimization to find the optimal cluster geometry was done with a steepest descent method. The convergence criteria were that the maximum force magnitude on any particle is less than 0.0005 hartree/bohr (hartree = 2 Ry ≈ 27.211 eV, bohr = a_0 ≈ 0.529 Å) and that the average over all particles is less than 0.00025 hartree/bohr. For further details, see sections S.1 and S.2 of the Supporting Information.

The SDFT-based calculation methodology used here in the first study on $Fe_xS_x^+$ (x = 2−4) clusters (ground state and higher energy isomers) and their binding to N_2 as well as that employed earlier in our joint experimental/theoretical investigations of manganese oxide clusters[37] have yielded results in agreement with literature data (see the SI) as well as with the information extracted from the present measurements (see below) and have led to a consistent interpretation of the current ion-trap experiments. The results of these calculations could be used in further comparative computational studies employing other methodologies devised for investigations of spin-coupled systems and antiferromagnetic configurations see, e.g., refs 38−42 and references cited therein.

3. RESULTS AND DISCUSSION

3.1. Model System. The core of the natural FeMo cofactor comprises two partial cubane clusters, Fe_4S_3 and $MoFe_3S_3$, which are bridged by three sulfide atoms and a 6-fold

DOI: 10.1021/acs.jpcc.6b02821
J. Phys. Chem. C XXXX, XXX, XXX−XXX

coordinated carbon atom as displayed in Figure 1a. This metal cluster core is bound to the protein by several hydrogen-bond

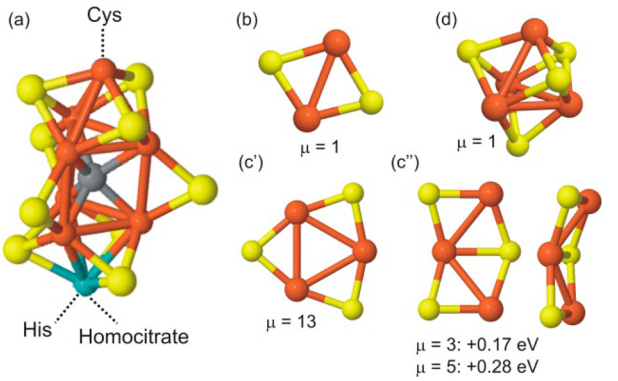

Figure 1. (a) Scheme of the active core of the natural nitrogenase FeMo-cofactor from *A. vinelandii* in the resting state (PDB entry 3U7Q on the basis of ref 10) and (b, c′, d) optimized structures of the biomimetic gas phase clusters $Fe_2S_2^+$, $Fe_3S_3^+$, and $Fe_4S_4^+$ as well as (c″) the first isomeric structure of $Fe_3S_3^+$. Further information about the ground state and isomeric configurations are given in Figures S2−S8. Fe, S, Mo, and C atoms are depicted as brown, yellow, blue, and gray spheres. The difference between the number of spin-up and spin-down electrons is given by μ; spin related values are expressed as 0.5μ. Here, as well as in the rest of the paper, we draw a line between neighboring Fe atoms. In the theoretically predicted structure figures displayed here, as well as elsewhere in this paper, the lines drawn between neighboring atoms indicate bonds, except those between neighboring Fe atoms; Fe−Fe indicates interaction between the Fe atoms but not necessarily formation of a real chemical bond.

interactions as well as no more than three covalently bound ligands: a homocitrate entity and a histidine residue are attached to the Mo atom, while one cysteine residue is attached to the opposite Fe atom.[6−10,43]

Although the geometrical structure of the FeMo cofactor has been very well resolved, the electronic structure is still the subject of an ongoing discussion.[44−50] A recent experimental study reassigned the formal oxidation state of the Mo atom in the resting state of the FeMo cofactor to +III (instead of +IV) resulting in three different models for the formal oxidation states of the Fe atoms.[47−49] Only lately, Spatzal et al. were able to provide the first comprehensive picture of the electron distribution in the FeMo cofactor.[50] Through use of spatially resolved X-ray diffraction, the oxidation states have been assigned to Mo(III)3Fe(II)4Fe(III), which results in a total charge of the $MoFe_7S_9C$ cluster of −1. However, no information is available so far about the electronic structure of the reduced N_2 binding state E_4H_4.

In this paper, free iron−sulfur clusters $Fe_2S_2^+$, $Fe_3S_3^+$, and $Fe_4S_4^+$ (shown in Figure 1b−d) are employed. Although these clusters represent simplified biomimetic systems which do not fully account for the complexity of the natural FeMo cofactor, joined experimental and theoretical studies of these systems can provide a conceptual understanding of the interaction of N_2 with iron−sulfur clusters. These model systems have been chosen on the basis of the following considerations:

(1) The model systems must, on the one hand, be simple enough to allow for a fundamental molecular level insight, while on the other hand, they must be complex enough to appropriately model the active center of the FeMo cofactor; i.e., they must contain more than one iron and sulfur atom.

(2) The model system must provide insight into the importance of the Fe atom coordination as well as structurally different adsorption sites such as Fe corners and FeS faces. This requirement is met by the investigation of three different cluster sizes and thus a gradual increase of the model system's complexity.

(3) Consideration of several findings pertaining to the role of the highly coordinated Mo atom in the FeMo factor indicates that N_2 may bind preferably to Fe atoms instead of to the Mo atom.[16,17,51] These findings include the ones showing that the substitution of Mo by V and Fe (in the alternative nitrogenase) reduces its reactivity but does not inhibit entirely its activity for N_2 reduction, as well as the finding that the influence of the identity of the additional metal atom (i.e., Mo or V) on substrate binding at Fe is only of secondary importance. Consequently, in a first step, the active cluster can be adequately modeled by a bare iron−sulfur cluster without an additional heterometal atom.

(4) Although the direct ligand environment of the metal cluster core is rather simple, it will likely influence the catalytic properties of the cluster. However, to gain conceptual understanding of the interaction between N_2 and iron−sulfur clusters (without addressing the complete catalytic ammonia synthesis mechanism), this ligand environment as well as the potential effects of the polar protein environment and the protons adsorbed at the FeMo cofactor are omitted in the free cluster model systems employed in this study. Whereas these model systems do not account for certain complex features of the FeMo cofactor, they do allow investigations of the intrinsic properties of the iron−sulfur clusters, thereby providing indispensable information for the development of biomimetic heterogeneous catalysts.

(5) The formal Fe oxidation states in the resting state of the FeMo cofactor have been assigned to +II and +III, while the electronic structure of the reduced N_2 binding state is not clear yet. The chosen gas phase clusters can be formally described by Fe(II)−Fe(III) for $Fe_2S_2^+$, 2Fe(II)−Fe(III) for $Fe_3S_3^+$, and 3Fe(II)−Fe(III) for $Fe_4S_4^+$; thus, they share the same formal oxidation states with the iron atoms in the known resting state of the FeMo cofactor.

The cationic $Fe_2S_2^+$ cluster (Figure 1b) has a rhombic ground-state structure with Fe−Fe and Fe−S bond lengths of d(Fe−Fe) = 2.7 Å and d(Fe−S) = 2.3 Å (2.3 Å) and exhibits a configuration with μ = 1. The corresponding isomer with μ = 7 is 0.54 eV higher in energy (compared to a previously reported[52] value of 0.42 eV).

The lowest energy structure of $Fe_3S_3^+$ (Figure 1c′) comprises an equilateral triangle formed by the Fe atoms with an Fe−Fe bond lengths of 2.9 Å. Each of the three edges of the triangle is bridged by one sulfur atom yielding an Fe−S bond length of 2.2 Å. This cluster has μ = 13 unpaired d-electrons. The first two higher energy isomeric structures (Figure 1c″) are distorted and bent incomplete hexagons. The first isomer has μ = 3 and is +0.17 eV higher in energy, whereas the second isomer has μ = 5 and is +0.28 eV higher in energy than the minimum energy structure. For the μ = 5 isomer, the Fe−Fe bond lengths are

DOI: 10.1021/acs.jpcc.6b02821
J. Phys. Chem. C XXXX, XXX, XXX−XXX

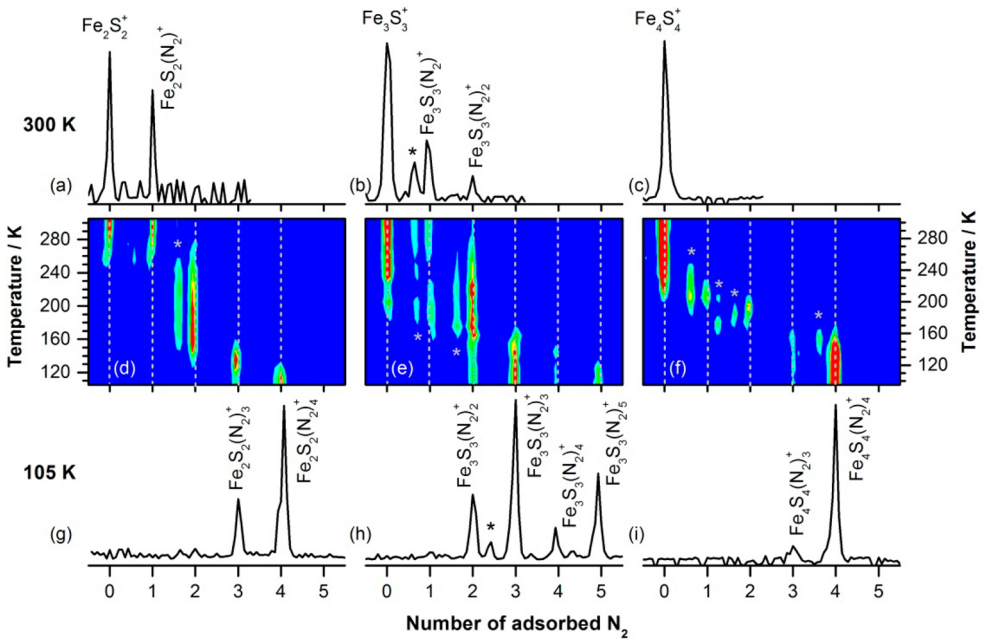

Figure 2. Ion mass distributions obtained after reaction of (a) $Fe_2S_2^+$, (b) $Fe_3S_3^+$, and (c) $Fe_4S_4^+$ with N_2 at room temperature. (d–f) 2D contour plot representation of the temperature-dependent ion mass distributions recorded in steps of 10 K after storing the clusters for 0.1 s in the ion tap. The relative ion intensity is color coded from blue (0%) to red (100%). (g–i) Corresponding ion mass distributions obtained at the lowest investigated reaction temperature of 105 K. $Fe_2S_2^+$: $p(He) = 0.94 \pm 0.05$ Pa, $p(N_2) = 0.14 \pm 0.01$ Pa; $Fe_3S_3^+$: $p(He) = 0.94 \pm 0.02$ Pa, $p(N_2) = 0.07 \pm 0.01$ Pa; $Fe_4S_4^+$: $p(He) = 0.98 \pm 0.04$ Pa, $p(N_2) = 0.14 \pm 0.01$ Pa. The products labeled with an asterisk are due to nonbakeable water impurities present in the experiment.

calculated to be 2.57, 2.76, and 3.86 Å and the average Fe–S bond length is 2.30 Å.

The largest studied model, $Fe_4S_4^+$, exhibits a cubelike structure with d(Fe–Fe) = 2.82 Å, d(Fe–S) = 2.38 Å, and a low ($\mu = 1$) electronic configuration. The isomer with $\mu = 17$ is +0.24 eV higher in energy. This represents the first investigation of the geometric and electronic structure of the bare cationic tetrairon–tetrasulfur cluster; however, a comparable cubic geometry has also been considered for ligated $Fe_4S_4^+$ and $Fe_4S_4^{2+}$ clusters.[53−56]

The optimized geometric motifs of the cationic clusters are retained for the corresponding neutral clusters. However, the minimum energy structures exhibit $\mu = 8$, 4, and 16 for Fe_2S_2, Fe_3S_3, and Fe_4S_4, respectively. The geometries of the neutral Fe_2S_2 and Fe_4S_4 are in agreement with previously found structures, while there is, however, no general agreement on the spin ground state.[52,57,58] The neutral Fe_3S_3 has previously been reported to have a more compact three-dimensional structure.[57] Further details about the calculated ground and isomeric cationic and neutral clusters are given in Figures S2–S9.

3.2. Temperature Dependent Adsorption of N_2. To gain insight into the reactive properties of our free cluster model systems, we have performed temperature-dependent reactivity experiments in an ion trap. Under the given experimental conditions, reactions between a cationic cluster and a neutral molecule are typically characterized by a negative temperature dependence; i.e., the rate constant increases with decreasing temperature. This behavior arises from the fact that the primary adsorption reaction between the cluster and the reactant follows the Lindemann energy transfer model for association reactions and usually occurs without an activation barrier.[59,60] Consequently, products observed at room temperature must contain more strongly bound ligands, while products with weakly bound ligands are only observed at lower temperatures (more details of the temperature dependence of reactions in the ion trap are given in section S.4 of the SI).

Figure 2 displays temperature-dependent ion mass distributions obtained after the reaction of $Fe_2S_2^+$, $Fe_3S_3^+$, and $Fe_4S_4^+$ with 0.14 Pa ($Fe_2S_2^+$ and $Fe_4S_4^+$) and 0.07 Pa ($Fe_3S_3^+$) N_2, respectively, for 0.1 s in the ion trap. $Fe_2S_2^+$ adsorbs one nitrogen molecule to form $Fe_2S_2(N_2)^+$ (Figure 2a), while $Fe_3S_3^+$ adsorbs up to two nitrogen molecules yielding $Fe_3S_3(N_2)^+$ and $Fe_3S_3(N_2)_2^+$ at room temperature (Figure 2b). In contrast, $Fe_4S_4^+$ does not react with N_2 at room temperature (Figure 2c). Even after longer reaction times of up to 1 s no reaction products are observed. Thus, $Fe_3S_3^+$ appears to be the most reactive cluster size at room temperature.

Cooling down the ion trap leads to the formation of additional reaction products. The smallest investigated cluster $Fe_2S_2^+$ adsorbs a second nitrogen molecule at a temperature of about 280 K. $Fe_2S_2(N_2)_2^+$ represents the main reaction product over a wide temperature range, and two more N_2 molecules are only adsorbed at temperatures as low as 150 and 130 K, respectively, yielding $Fe_2S_2(N_2)_3^+$ and $Fe_2S_2(N_2)_4^+$. Similarly, $Fe_3S_3(N_2)_2^+$ is found to be the main reaction product over a wide temperature range. However, this cluster adsorbs up to three more nitrogen molecules at lower temperatures to form $Fe_3S_3(N_2)_3^+$ at about 180 K, $Fe_3S_3(N_2)_4^+$ at about 150 K and $Fe_3S_3(N_2)_5^+$ at about 130 K. These temperature-dependent product formations indicate the rather strong binding of the first two N_2 molecules, while the adsorption of further multiple N_2 molecules at cryogenic temperatures suggests a more weakly binding of these N_2 molecules. In marked contrast, for $Fe_4S_4^+$ the formation of a first adsorption product, $Fe_4S_4(N_2)^+$, after a reaction time of 0.1 s requires a temperature below about 230 K. Up to three more nitrogen molecules are adsorbed at even lower temperatures, yielding $Fe_4S_4(N_2)_2^+$ at about 210 K as well

DOI: 10.1021/acs.jpcc.6b02821
J. Phys. Chem. C XXXX, XXX, XXX–XXX

as $Fe_4S_4(N_2)_3^+$ and $Fe_4S_4(N_2)_4^+$ at about 170 K. Apart from the presented $Fe_xS_x(N_2)_y^+$ products, all three cluster sizes show additional reaction products (marked with an asterisk) which arise from the competing reaction with nonbakeable trace amounts of water (i.e., which cannot be removed by heating the gas lines and the ion trap) and will thus not be further discussed here.

In summary, these temperature-dependent experiments show that all three investigated clusters are able to adsorb N_2. Thus, they can be regarded as the first multiiron−multisulfur clusters which are able to bind N_2. We note here that in all of the above examples the N_2 molecule attaches to the iron−sulfide clusters nondissociatively. This is supported by the first-principle calculated total energy difference between the molecularly adsorbed state and the dissociated one for $Fe_4S_4^+$ cluster, i.e., $E[Fe_4S_4^+(2N)] - E[(Fe_4S_4^+(N_2)] = 7.83$ eV; therefore, it is predicted that dissociation of the adsorbed N_2 molecule would entail a prohibitive energetic cost. Theoretical results pertaining to the binding of single and multiple N_2 molecules to the iron−sulfur clusters investigated in this work, yielding results in agreement with the measurements and elucidating the structures of the nitrogen adsorbed complexes and the binding mode of the molecule to the cluster, are discussed in the following section.

3.3. Bond Strength and Binding Geometry of N_2.

Previously, the bond strength and binding geometry of N_2 to iron−sulfur surfaces and several isolated model systems have almost exclusively been investigated theoretically. One experimental study addressed the adsorption of N_2 on a single-crystal pyrite $FeS_2(100)$ surface. N_2 has been found to adsorb only at temperatures lower than 130 K, and the surface species has been identified as chemisorbed molecular N_2.[61] The experimentally found low adsorption temperature contrasts, however, with DFT calculations which predicted a rather high binding energy of 0.99 eV for N_2 adsorbed with the molecular axis almost perpendicular to the $FeS_2(100)$ surface, whereas parallel binding was not found to be stable.[62] A second experimental study presented the synthesis of a monoiron−disulfur complex which binds a nitrogen molecule via terminal coordination to the iron atom. In this complex, the N−N bond length has been found to be 1.13 Å; nevertheless, the nitrogen bound complex appeared to be thermally very sensitive and N_2 coordination was only observed at temperatures well below room temperature.[27] In agreement, spectroscopic studies on trapped intermediates of the biological FeMo cofactor also indicated the terminal (end-on) binding of N_2.[20,21]

In contrast to the limited investigations on iron−sulfur surfaces, isolated model systems have been studied theoretically in more detail by several groups. These model systems range from simple monoiron complexes[63,64] to more complicated structures containing multiple iron atoms[65] and to bare and ligated clusters comprising a molybdenum heteroatom such as $MoFe_7S_9$ or $MoFe_7S_9X$.[66−70] Some studies predict the binding of N_2 via coordination to several (two or three) iron atoms,[65,66,71] whereas others find the preferred binding of N_2 to be in an end-on configuration.[63,64,70] Most interestingly, even for the more complex model systems containing a molybdenum heteroatom, end-on binding of N_2 to Fe has been observed to be more favorable.[17,67−69] Depending on the exact model and the level of theory used, the predicted N_2 binding energies vary over a wide range between 0.1 and 1.38 eV. One publication even reported an extremely high value of 6.5 eV for N_2 binding to $MoFe_7S_9$ cluster core with 39 d electrons, which corresponds to the resting state.[66]

Because currently most investigations are theoretical in nature and there is a controversy pertaining to the interaction between N_2 and iron−sulfur clusters, it is highly desirable to obtain detailed experimental data on these systems, coupled with coordinated theoretical analysis. In section 3.2, we have demonstrated that free iron−sulfur clusters $Fe_xS_x^+$ (x = 2−4) represent multiiron−multisulfur clusters which are able to bind N_2. To quantify the reaction of these free iron−sulfur clusters with N_2, kinetic measurements have been performed at selected reaction temperatures. As an example, Figure 3 displays

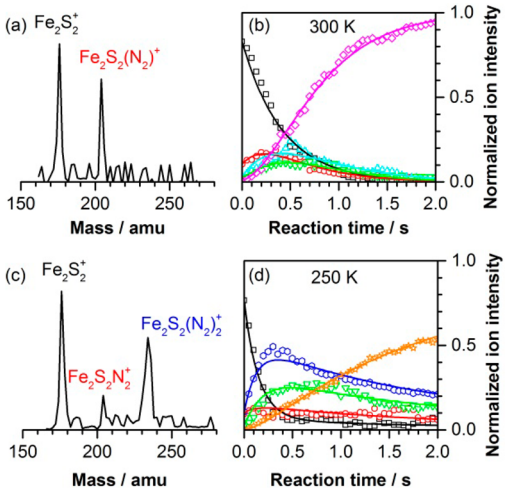

Figure 3. Ion mass distributions and corresponding kinetic data obtained at two selected temperatures of 300 K (a,b) and 250 K (c,d), respectively. The open symbols represent the experimental data, normalized to the total ion concentration in the ion trap. The solid lines are obtained by fitting the integrated rate equations of proposed reaction mechanisms (see section S.5 of the SI). (a,b) p(He) = 1.00 ± 0.01 Pa, $p(N_2)$ = 0.11 ± 0.01 Pa; (c,d) p(He) = 0.98 ± 0.01 Pa, $p(N_2)$ = 0.09 ± 0.01 Pa. □: $Fe_2S_2^+$, ○: $Fe_2S_2(N_2)^+$, ⬠: $Fe_2S_2(N_2)_2^+$, △: $Fe_2S_2(H_2O)^+$, ▽: $Fe_2S_2(N_2)(H_2O)^+$, ◇: $Fe_2S_2(H_2O)_2^+$, ☆: $Fe_2S_2(H_2O)_3^+$.

representative mass spectra and the corresponding kinetic data obtained after the reaction of $Fe_2S_2^+$ with N_2 at 300 and 250 K, respectively. The shown mass spectra were recorded after a reaction time of 0.1 s and show signals corresponding to the bare cluster $Fe_2S_2^+$ and the adsorption complexes $Fe_2S_2(N_2)^+$ and $Fe_2S_2(N_2)_2^+$. At longer reaction times (not shown here), additional water containing products are observed. For completeness, the traces of these products are also shown in the kinetic data.

The normalized kinetic data were evaluated by fitting integrated rate equations of potential sequential adsorption mechanisms to the experimental data. The simplest reaction mechanism that best fits the experimental kinetic data at room temperature is given by

$$Fe_2S_2^+ + N_2 \rightleftarrows Fe_2S_2(N_2)^+ \quad (1a)$$

$$Fe_2S_2(N_2)^+ + H_2O \rightleftarrows Fe_2S_2(N_2)(H_2O)^+ \quad (1b)$$

$$Fe_2S_2(N_2)(H_2O)^+ \rightleftarrows Fe_2S_2(H_2O)^+ + N_2 \quad (1c)$$

$$Fe_2S_2(H_2O)^+ + H_2O \rightarrow Fe_2S_2(H_2O)_2^+ \quad (1d)$$

DOI: 10.1021/acs.jpcc.6b02821
J. Phys. Chem. C XXXX, XXX, XXX−XXX

The simplest reaction mechanism that best fits the experimental kinetic data at 250 K is

$$Fe_2S_2^+ + N_2 \rightleftarrows Fe_2S_2(N_2)^+ \quad (2a)$$

$$Fe_2S_2(N_2)^+ + N_2 \rightleftarrows Fe_2S_2(N_2)_2^+ \quad (2b)$$

$$Fe_2S_2(N_2)^+ + H_2O \rightleftarrows Fe_2S_2(N_2)(H_2O)^+ \quad (2c)$$

$$Fe_2S_2(N_2)(H_2O)^+ + 2H_2O \rightleftarrows Fe_2S_2(H_2O)_3^+ + N_2 \quad (2d)$$

The experimental data are shown as open symbols in Figure 3b,d, while the solid lines are obtained by the fitting procedure. This not only leads to the determination of the simplest reaction mechanism that best fits the experimental data but in this case more importantly to the corresponding rate constants. The fitting procedure yields a termolecular rate constant $k^{(3)}$ for the adsorption of a first N_2 molecule to $Fe_2S_2^+$ of $(2.2 \pm 0.4) \times 10^{-28}$ cm^6 s^{-1} at 300 K and $(12.3 \pm 2.6) \times 10^{-28}$ cm^6 s^{-1} at 250 K, respectively. These temperature-dependent rate constants in conjunction with the Lindemann energy transfer model for association reactions[59,60,72] and the statistical unimolecular reaction rate theory in the framework of the RRKM (Rice−Ramsperger−Kassel−Marcus) model[73] can be used to determine the $Fe_2S_2^+$−N_2 binding energy[60] (details of this procedure are given in section S.6 of the SI). The resulting binding energy of a first N_2 molecule to $Fe_2S_2^+$ amounts to 0.84 ± 0.10 eV. Employing the same procedure to the larger clusters yields N_2 binding energies of 0.72 ± 0.10 eV for $Fe_3S_3^+$ and 0.50 ± 0.10 eV for $Fe_4S_4^+$ as illustrated in Figure 4.

Figure 4 also displays the optimized structures of the complexes $Fe_xS_x(N_2)^+$. For all studied cluster sizes, N_2 is found to bind molecularly to one of the Fe atoms in an end-on configuration. The Fe−N distance amounts to 2.1 Å for $Fe_2S_2^+$ and $Fe_3S_3^+$ and is slightly elongated to 2.26 Å for $Fe_4S_4^+$. First, we note the antiferromagnetic configurations for the ground states of these cationic clusters. The N−N distance of the free N_2 molecule is calculated to be 1.11 Å, and it remains unchanged upon adsorption on the clusters. Thus, despite the increasing complexity of the employed clusters and the availability of different adsorption sites, the binding geometry and the electronic interaction appear to be cluster size independent.

In the case of $Fe_2S_2^+$ and $Fe_4S_4^+$, neither the geometry nor the spin state of the cluster core is affected by the adsorption of N_2 as can be seen by a comparison of parts b and d of Figure 1 with Figure 4. The isomer with $\mu = 7$ of $Fe_2S_2(N_2)^+$ is found to be +0.59 eV higher in energy and the isomer with $\mu = 17$ of $Fe_4S_4(N_2)^+$ is +0.29 eV higher in energy than the corresponding ground-state isomers with $\mu = 1$. The energy differences between the ground-state structures of $Fe_2S_2^+$ and $Fe_2S_2(N_2)^+$ as well as of $Fe_4S_4^+$ and $Fe_4S_4(N_2)^+$ amount to 0.83 and 0.47 eV, respectively, which are in good agreement with the experimentally obtained N_2 binding energies of 0.84 ± 0.1 and 0.50 ± 0.10 eV. In contrast, the situation is more complex for $Fe_3S_3^+$. The FeS core of the $Fe_3S_3(N_2)^+$ ground state structure is a distorted incomplete hexagon with $\mu = 5$. Thus, upon adsorption of N_2, both the cluster geometry and the spin-state change. The energy difference between the ground state structure of $Fe_3S_3^+$ (planar S-bridged triangle, $\mu = 13$, cf. Figure 1c′) and $Fe_3S_3(N_2)^+$ (incomplete hexagon, $\mu = 5$, cf. Figure 4) amounts to 0.53 eV which is considerably lower than the experimentally obtained N_2 binding energy of 0.72 ± 0.10 eV.

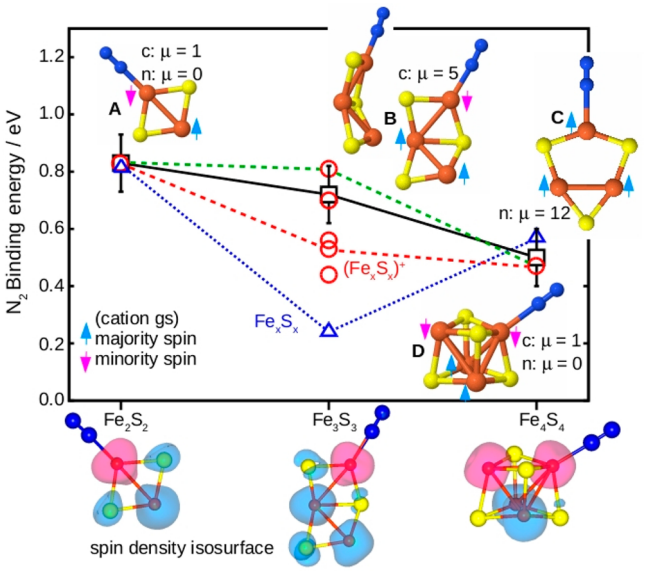

Figure 4. Cluster size dependent experimental (black squares) and theoretical (red circles) binding energies of N_2 to cationic $Fe_xS_x^+$ (x = 2−4) as well as theoretical binding energies of N_2 to neutral Fe_xS_x (x = 2−4) (blue triangles). All lines are drawn to guide the eye. The red (blue) lines connect the values obtained for the ground state isomers of the bare cluster and the charged $Fe_xS_x(N_2)^+$ (neutral $Fe_xS_x(N_2)$) complex, respectively, while the remaining theoretical values (red circles) are obtained for higher energy isomers of the bare cluster and/or the formed complex (more details are given in the text). The green line connects the (calculated) transitions between ground-state $Fe_xS_x(N_2)^+$ and the bare $Fe_xS_x^+$ cluster which has the same number of unpaired electrons, μ, and structure. Also shown are the optimized geometric structures of the cationic (c) $Fe_xS_x(N_2)^+$ (x = 2−4) as well as the neutral (n) $Fe_3S_3(N_2)$. Fe, S, and N atoms are depicted as red, yellow, and blue spheres. The locations and spatial distributions of the majority (blue, up-arrows) and minority (purple, down-arrows) spin densities for the ground states of the cationic $Fe_xS_x(N_2)^+$ (x = 2−4) clusters are shown in the upper insets and at the bottom of the figure, respectively. The majority (blue) and minority (purple) spin distributions (depicted by the 90% isosurfaces at the bottom of the figure) were obtained from the difference between the calculated total majority spin and minority spin densities of the clusters. The antiferromagnetic configurations of the cationic clusters are evident; note the ferromagnetic configuration of the neutral $Fe_3S_3(N_2)$ cluster.

Most interestingly, the cluster core of $Fe_3S_3(N_2)^+$ is a distorted incomplete hexagon which corresponds to the structure of the first two higher energy isomers of the bare $Fe_3S_3^+$ cluster (cf. Figure 1c″). The discrepancy between the experimental and theoretical binding energy could be explained by (1) an energy barrier for the structural transformation of the cluster core (see Figure S8) or (2) contributions from higher energy isomers. In the first case, the models employed for the determination of the experimental binding energies are too simple and cannot account for the more complex temperature dependence of the rate constants. Consequently, the determined binding energy is not reliable anymore. Such a scenario cannot be excluded for N_2 binding to $Fe_3S_3^+$ (a more detailed discussion is given in section S.6 of the SI).

To evaluate the possibility of the second case, we also show theoretical binding energies (red circles) obtained for higher energy isomers of the bare cluster and/or the formed complex in Figure 4. In particular, the energy differences between the first two higher energy isomers of the bare $Fe_3S_3^+$ (incomplete hexagon, $\mu = 3$, $\delta E = +0.17$ eV and incomplete hexagon, $\mu = 5$,

DOI: 10.1021/acs.jpcc.6b02821
J. Phys. Chem. C XXXX, XXX, XXX−XXX

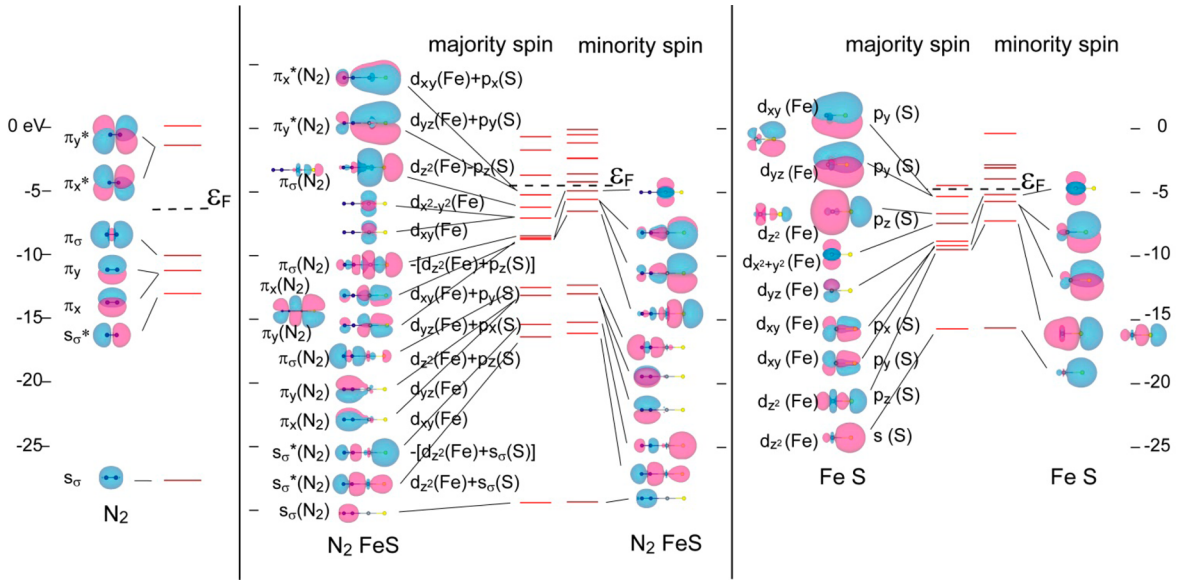

Figure 5. Electronic structure and orbital isosurfaces (with positive and negative values depicted in blue and pink, respectively) for a free N_2 molecule (left panel), FeS (right panel), and the $FeSN_2$ complex (middle panel). The electronic states are shown separately for the up and down spin manifolds. Understanding the bonding of N_2 to FeS is facilitated by correlating the right and left panels with the orbital scheme of the $FeSN_2$ complex in the middle panel.

δE = +0.28 eV) shown in Figure 1c″ and the ground-state structure of $Fe_3S_3(N_2)^+$ (incomplete hexagon, μ = 5) are 0.70 and 0.81 eV, respectively (see Figure S6), which agrees favorably with the experimentally obtained value of 0.72 ± 0.10 eV. Thus, a closer agreement with the experiment is obtained when in the theory the ground state cluster complex with nitrogen ($Fe_3S_3(N_2)^+$) and the bare cluster after nitrogen removal have the same geometry (i.e., incomplete hexagon with μ = 5). Since these two isomers (of the bare cluster) are calculated to be only +0.17 and +0.28 eV higher in energy than the ground-state structure, contributions of these clusters in the experiment cannot be excluded.

For comparison, we have also theoretically explored the binding of N_2 to neutral Fe_xS_x. For all investigated clusters, the structural motif of the cluster core is retained upon adsorption of N_2 and N_2 binds as an intact (not dissociated) molecule to one of the Fe atoms in an end-on configuration. Consequently, the geometries of $Fe_2S_2(N_2)$ and $Fe_4S_4(N_2)$ are similar to the ones for the corresponding cationic clusters (cf. Figure 4, structures A and D), while $Fe_3S_3(N_2)$ is a planar S-capped triangle (cf. Figure 4, structure C). The energy differences between the ground-state structures of the bare Fe_xS_x clusters and the ground-state structures of the complexes $Fe_xS_x(N_2)$ amount to 0.83 eV (Fe_2S_2), 0.24 eV (Fe_3S_3), and 0.57 eV (Fe_4S_4). Thus, N_2 binding energies for triiron−trisulfur cluster appear to be strongly charge-dependent, whereas in marked contrast, the values for Fe_2S_2 and for Fe_4S_4 are almost identical (more details are given in Figures S2−S4).

To this point we addressed theoretically single N_2 molecular adsorption on the iron−sulfur clusters. In the following, we discuss briefly the results of our first-principles calculations for multiple dinitrogen molecular adsorption. The ion mass distributions shown in Figure 2 for the $Fe_xS_x^+$ (x = 2−4) clusters after interaction with N_2 measured at temperatures ranging between 120 and 300 K indicate a dependence of the adsorption strength on the number of coadsorbed molecules and cluster-size-dependent variations in the adsorption strengths. The results of our calculations for $Fe_2S_2(N_2)_y^+$ and $Fe_4S_4(N_2)_y^+$ (y = 1−4) clusters are shown in Figure S10, and they are summarized in Table S1. For the $Fe_2S_2(N_2)_y^+$ cluster, we find the following binding energies (per molecule) for y = 1−4 N_2 molecules: BE(1) = 0.83 eV, BE(2) = 0.74 eV, BE(3) = 0.60 eV, BE(4) = 0.45 eV. For $Fe_4S_4(N_2)_y^+$, we find BE(1) = 0.54 eV, BE(2) = 0.46 eV, BE(3) = 0.48 eV, and BE(4) = 0.46 eV. Comparison of the calculated values with the measured data in Figure 2 reveals that the measured general trend of decreasing adsorption energies with increasing number of coadsorbed N_2 molecules is reproduced by the calculations. We also find that the rate of adsorption energy decrease depends on the cluster size (number of Fe atoms). Thus, for the smaller $Fe_2S_2^+$ cluster the N_2 adsorption energies drop sharply when the number of adsorbed molecules exceeds (i.e., for y > 2) the number of Fe atoms (x = 2) in the cluster (the adsorption energy of the fourth molecule $\delta(4)$ = 4BE(4) − 3BE(3) is calculated to be vanishingly small), whereas for the larger $Fe_4S_4^+$ cluster the adsorption energy of the fourth molecule remains finite, $\delta(4)$ = 0.40 eV.

We conclude this section by remarking that the observation of a molecular nondissociative binding of N_2 has also strong mechanistic implications for a possible subsequent conversion of N_2 to ammonia. Since N_2 does not dissociate on the cluster, hydrogen atoms must directly interact with the nitrogen molecule and NH_3 formation must proceed via successive formation of diazene N_2H_2 and hydrazine N_2H_4. Such a reaction mechanism has theoretically been proposed by several groups[65,68,74−76] and is also experimentally confirmed[13−15] for the biological nitrogen reduction. It is, however, in contrast to the mechanism proceeding on conventional industrial catalysts which involves the dissociation of N_2 and subsequent combination of surface adsorbed N and H atoms (see ref[76] and references therein). Further experimental and theoretical investigations in this direction are currently in progress in our laboratories.

3.4. Bonding Mechanism of N_2. To elucidate the nature of the interaction between the iron−sulfur clusters with N_2, the electronic structure has been investigated theoretically using the

DOI: 10.1021/acs.jpcc.6b02821
J. Phys. Chem. C XXXX, XXX, XXX−XXX

example of $FeSN_2$. The calculated orbital correlation diagram is shown in Figure 5 and illustrates the orbital scheme for the FeS molecule (right panel of the figure) and the way that this molecule combines with the nitrogen molecule (N_2, see orbital scheme in the left panel of Figure 5) to form the bound complex $FeSN_2$ (middle panel of Figure 5). An important contribution to the binding of N_2 to FeS is associated with the interaction of the unoccupied π_x^* and π_y^* antibonding levels of the N_2 molecule with the frontier orbitals (the highest occupied molecular orbitals, HOMO) of the FeS molecule, d_{xy}(Fe) + p_x(S) and d_{yz}(Fe) + p_y(S). This interaction drags the N_2 unoccupied orbitals below the Fermi energy level (ε_F) of the complex, resulting in their partial occupation by electrons of the FeS molecule. The partial occupation of the aforementioned antibonding orbitals weakens the internitrogen triple bond, thus promoting binding of the N_2 molecule to FeS to form the stably bonded $FeSN_2$ complex (an example of the bond-order conservation principle). Although the N−N bond length of the adsorbed N_2 molecules changes only slightly in the $FeSN_2$ complex (1.12 Å) compared to that in the free molecule (1.11 Å), the calculated N−N stretch frequency in the $FeSN_2$ complex (2158 cm^{-1}) is found to decrease more substantially compared to the calculated stretch frequency of N_2 (2324 cm^{-1}); the latter value compares well with the measured stretch frequency[77] of N_2, 2358 cm^{-1}. The interaction scheme described above by our first-principles calculations between the iron−sulfur cluster and N_2, involving weakening of the N−N bond, agrees well with the low N−N stretch frequency of only 1880 cm^{-1}, which has been measured for a recently synthesized monoiron−disulfur−N_2 complex.[27] We have calculated the N−N stretch frequencies for the N_2 molecule and for the neutral ground-state clusters with adsorbed N_2. The N−N stretch frequencies we obtain are 2324 cm^{-1} for the N_2 molecule (the experimental value[77] is 2358 cm^{-1}), 2255 cm^{-1} for $Fe_3S_3(N_2)$, and 2201 cm^{-1} for $Fe_4S_4(N_2)$. In contrast, the N−N stretch frequencies for the cationic clusters (for example 2315 cm^{-1} for $Fe_4S_4(N_2)^+$) are hardly changed from the free N_2 molecule.

4. CONCLUSION

To gain fundamental insights into the binding of N_2 to iron−sulfur clusters, we present a new and unique approach by employing free iron−sulfur clusters $Fe_2S_2^+$, $Fe_3S_3^+$, and $Fe_4S_4^+$ as model systems. Temperature-dependent kinetic measurements in an ion trap revealed that these clusters adsorb N_2 and thus represent the first cluster model systems comprising several iron and sulfur atoms, respectively, which are able to bind molecular nitrogen. Furthermore, we present for the first time experimentally obtained binding energies of N_2 to iron−sulfur clusters. Such experimental values are of particular importance since the interaction of N_2 with active iron−sulfur clusters has so far only been studied theoretically, and current findings have been the subject of debate and controversy.

Concurrent first-principles simulations provided molecular level understanding of the interaction between iron−sulfur clusters and N_2. Independent of the cluster size and the charge state of the cluster, N_2 is found to bind molecularly to one of the Fe atoms in an end-on configuration. Thus, this binding motif is not a peculiarity of the model system but can rather be regarded as a general concept. The binding of N_2 to the iron−sulfur clusters is found to be enabled by occupation of the empty antibonding π_x^* and π_y^* of the (free) N_2 molecule through interaction of the frontier HOMO orbitals of the iron−sulfur complex (involving d-orbitals of iron hybridized with sulfur p-orbitals). This weakens the strong triple bond of N_2 (bond-order reduction), promoting in turn binding of the molecule to the iron−sulfur complex.

These gas-phase model studies represent an import step toward a conceptual understanding of the interaction between the substrate N_2 and iron−sulfur clusters. This knowledge is expected to open new avenues for future experimental and theoretical investigations, aiming at elucidating details of the catalytic ammonia synthesis under ambient conditions. Moreover, this study can be considered as the first step of a bottom-up approach for the future design of biomimetic heterogeneous catalysts. Further steps of our working plan include the addition of molecular hydrogen to study a potential ammonia synthesis reaction as well as the addition of heterometal atoms and appropriate ligands to change and optimize the reactive properties.

■ ASSOCIATED CONTENT

Supporting Information

The Supporting Information is available free of charge on the ACS Publications website at DOI: 10.1021/acs.jpcc.6b02821.

Theoretical method and detailed information about neutral and cationic $Fe_xS_x^+$ and $Fe_xS_x(N_2)^+$ clusters, x = 2−4, in the ground state and isomeric forms (geometric and spin isomers); details on the data evaluation procedure (PDF)

■ AUTHOR INFORMATION

Corresponding Authors

*E-mail: sandra.lang@uni-ulm.de. Tel: +49-731-50-25505.
*E-mail: uzi.landman@physics.gatech.edu. Tel: +1-404-894-7747.

Notes

The authors declare no competing financial interest.

■ ACKNOWLEDGMENTS

We gratefully acknowledge financial support by the Deutsche Forschungsgemeinschaft and the DAAD. In particular, S.M.L. is grateful to the European Social Fund Baden-Württemberg for a Margarete von Wrangell fellowship. R.N.B. was supported by Grant No. FG05-86ER45234 from the Office of Basic Energy Sciences of the US Department of energy (DOE) and U.L. by the Air Force Office for Scientific Research (AFOSR). Computations were carried out at the Georgia Tech Center for Computational Materials Science.

■ REFERENCES

(1) Gates, B. C. *Catalytic Chemistry*; John Wiley & Sons: New York, 1992.
(2) Ertl, G. Reachtion Mechanisms in Catalysis by Metals. *Crit. Rev. Solid State Mater. Sci.* **1982**, *10*, 349−372.
(3) Lee, C. C.; Wiig, J. A.; Hu, Y.; Ribbe, M. W., Structures and Function of the Active Sites of Nitrogenases. In *Bioinspired Catalysis: Metal−Sulfur Complexes*; Weigand, W., Schollhammer, P., Eds.; Wiley−VCH: Weinheim, 2015; pp 201−224.
(4) Smith, B. E.; Richards, R. L.; Newton, W. E. *Catalysis for Nitrogen Fixation - Nitrogenases, Relevant Chemical Models and Commercial Processes*; Kluwer Academic Publisher: Dordrecht, 2004; Vol. *1*.
(5) Hu, Y.; Ribbe, M. W. Nitrogenase Assembly. *Biochim. Biophys. Acta, Bioenerg.* **2013**, *1827*, 1112−1122.

DOI: 10.1021/acs.jpcc.6b02821
J. Phys. Chem. C XXXX, XXX, XXX−XXX

(6) Kim, J.; Rees, D. C. Structural Models for the Metal Centers in the Nitrogenase Molybdenum-Iron Protein. *Science* **1992**, *257*, 1677−1682.
(7) Chan, M. K.; Kim, J.; Rees, D. C. The Nitrogenase FeMo-Cofactor and P-Cluster Pair: 2.2 Å Resolution Structures. *Science* **1993**, *260*, 792−794.
(8) Einsle, O.; Tezcan, F. A.; Andrade, S. L. A.; Schmid, B.; Yoshida, M.; Howard, J. B.; Rees, D. C. Nitrogenase MoFe-Protein at 1.16 Å Resolution: A Central Ligand in the FeMo-Cofactor. *Science* **2002**, *297*, 1696−1700.
(9) Lancaster, K. M.; Roemelt, M.; Ettenhuber, P.; Hu, Y.; Ribbe, M. W.; Neese, F.; Bergmann, U.; DeBeer, S. X-Ray Emission Spectroscopy Evidences a Central Carbon in the Nitrogenase Iron-Molybdenum Cofactor. *Science* **2011**, *334*, 974−977.
(10) Spatzal, T.; Aksoyoglu, M.; Zhang, L.; Andrade, S. L. A.; Schleicher, E.; Weber, S.; Rees, D. C.; Einsle, O. Evidence for Interstitial Carbon in Nitrogenase FeMo Cofactor. *Science* **2011**, *334*, 940.
(11) Hales, B. J., Vanadium Nitrogenase. In *Catalysts for Nitrogen Fixation: Nitrogenases, Relevant Chemical Models, and Commercial Processes*; Smith, B. E., Richards, R. L., Newton, W. E., Eds.; Kluwer Academic Press: Dordrecht, 2004; pp 255−279.
(12) Schneider, K.; Müller, A., Iron-Only Nitrogenase: Exceptional Catalytic, Structural and Spectroscopic Features. In *Catalysts for Nitrogen Fixation: Nitrogenases, Relevant Chemical Models, and Commercial Processes*; Smith, B. E., Richards, R. L., Newton, W. E., Eds.; Kluwer Academic Publishers: Dordrecht, 2004; pp 281−307.
(13) Hoffman, B. M.; Lukoyanov, D.; Yang, Z.-Y.; Dean, D. R.; Seefeldt, L. C. Mechanism of Nitrogen Fixation by Nitrogenase: The Next Stage. *Chem. Rev.* **2014**, *114*, 4041−4062.
(14) Seefeldt, L. C.; Hoffman, B. M.; Dean, D. R. Mechanism of Mo-Dependent Nitrogenase. *Annu. Rev. Biochem.* **2009**, *78*, 701−722.
(15) Hoffman, B. M.; Dean, D. R.; Seefeldt, L. C. Climbing Nitrogenase: Toward a Mechanism of Enzymatic Nitrogen Fixation. *Acc. Chem. Res.* **2009**, *42*, 609−619.
(16) Seefeldt, L. C.; Dance, I. G.; Dean, D. R. Substrate Interactions with Nitrogenase: Fe Versus Mo. *Biochemistry* **2004**, *43*, 1401−1409.
(17) Dance, I. Activation of N_2, the Enzymatic Way. *Z. Anorg. Allg. Chem.* **2015**, *641*, 91−99.
(18) Igarashi, R. Y.; Seefeldt, L. C. The Mechanism of Mo-Dependent Nitrogenase: Thermodynamics and Kinetics. In *Catalysts for Nitrogen Fixation: Nitrogenases, Relevant Chemical Models, and Commercial Processes*; Smith, B. E., Richards, R. L., Newton, W. E., Eds.; Kluwer Academic Publishers: Dordrecht, 2004; pp 97−140.
(19) Henderson, R. A. Mechanistic Studies on Synthetic Fe-S-Based Clusters and Their Relevance to the Action of Nitrogenase. *Chem. Rev.* **2005**, *105*, 2365−2437.
(20) Barney, B. M.; Yang, T.-C.; Igarashi, R. Y.; Santos, P. C. D.; Laryukhin, M.; Lee, H.-I.; Hoffman, B. M.; Dean, D. R.; Seefeldt, L. C. Intermediates Trapped During Nitrogenase Reduction of N-N, CH_3-N-NH, and H_2N-NH_2. *J. Am. Chem. Soc.* **2005**, *127*, 14960−14961.
(21) Barney, B. M.; Lukoyanov, D.; Igarashi, R. Y.; Laryukhin, M.; Yang, T.-C.; Dean, D. R.; Hoffman, B. M.; Seefeldt, L. C. Trapping an Intermediate of Dinitrogen (N_2) Reduction on Nitrogenase. *Biochemistry* **2009**, *48*, 9094−9102.
(22) Barriere, F.; Durrant, M. C.; Pickett, C. J., Chemical Models, Theoretical Calculations, and the Reactivity of Isolated Iron-Molybdenum Cofactors. In *Catalysts for Nitrogen Fixation: Nitrogenases, Relevant Chemical Models, and Commercial Processes*; Smith, B. E., Richards, R. L., Newton, W. E., Eds.; Kluwer Acamdemic Publishers: Dordrecht, 2004; pp 161−199.
(23) Crossland, J. L.; Tyler, D. R. Iron-Dinitrogen Coordination Chemistry: Dinitrogen Activation and Reactivity. *Coord. Chem. Rev.* **2010**, *254*, 1883−1894.
(24) MacLeod, K. C.; Holland, P. L. Recent Developments in the Homogeneous Reduction of Dinitrogen by Molybdenum and Iron. *Nat. Chem.* **2013**, *5*, 559−564.
(25) Hazari, N. Homogeneous Iron Complexes for the Conversion of Dinitrogen into Ammonia and Hydrazine. *Chem. Soc. Rev.* **2010**, *39*, 4044−4056.
(26) Henderson, R. A., Binding Substrates to Synthetic Fe-S-Based Clusters and the Possible Relevance to Nitrogenases. In *Bioinspired Catalysis: Metal-Sulfur Complexes*; Weigand, W., Schollhammer, P., Eds.; Wiley−VCH: Weinheim, 2015; pp 289−323.
(27) Čorić, I.; Mercado, B. Q.; Bill, E.; Vinyard, D. J.; Holland, P. L. Binding of Dinitrogen to an Iron-Sulfur-Carbon Site. *Nature* **2015**, *526*, 96−99.
(28) Nakajima, A.; Hayase, T.; Hayakawa, F.; Kaya, K. Study on Iron-Sulfur Cluster in Gas Phase: Electronic Structure and Reactivity. *Chem. Phys. Lett.* **1997**, *280*, 381−389.
(29) Koszinowski, K.; Schröder, D.; Schwarz, H. Formation and Reactivity of Gaseous Iron-Sulfur Clusters. *Eur. J. Inorg. Chem.* **2004**, *2004*, 44−50.
(30) Heim, H. C.; Bernhardt, T. M.; Lang, S. M. The Challenge of Genrating Iron-Sulfur Clusters. *Int. J. Mass Spectrom.* **2015**, *387*, 56−59.
(31) Keller, R.; Nöhmayer, F.; Spädtke, P.; Schönenberg, M. H. CORDIS - an Improved High-Current Ion Source for Gases. *Vacuum* **1984**, *34*, 31−35.
(32) Bernhardt, T. M. Gas-Phase Kinetics and Catalytic Reactions of Small Silver and Gold Clusters. *Int. J. Mass Spectrom.* **2005**, *243*, 1−29.
(33) Lang, S. M.; Fleischer, I.; Bernhardt, T. M.; Barnett, R. N.; Landman, U. Low Temperature CO Oxidation Catalyzed by Free Palladium Clusters: Similarities and Differences to Pd Surfaces and Supported Particles. *ACS Catal.* **2015**, *5*, 2275.
(34) Barnett, R. N.; Landman, U. Born-Oppenheimer Molecular-Dynamics Simulations of Finite Systems: Structure and Dynamics of $(H_2O)_2$. *Phys. Rev. B: Condens. Matter Mater. Phys.* **1993**, *48*, 2081−2097.
(35) Troullier, N.; Martins, J. L. Efficient Pseudopotentials for Plane-Wave Calculations. *Phys. Rev. B: Condens. Matter Mater. Phys.* **1991**, *43*, 1993−2006.
(36) Perdew, J. P.; Burke, K.; Ernzerhof, M. Generalized Gradient Approximation Made Simple. *Phys. Rev. Lett.* **1996**, *77*, 3865−3868.
(37) Lang, S. M.; Bernhardt, T. M.; Kiawi, D. M.; Bakker, J. M.; Barnett, R. N.; Landman, U. The Interaction of Water with Free $Mn_4O_4^+$ Clusters: Deprotonation and Adsorption-Induced Structural Transformations. *Angew. Chem.* **2015**, *127*, 15328−15332.
(38) Noodleman, L. Valence Bond Description of Antiferromagnetic Coupling in Transition Metal Dimers. *J. Chem. Phys.* **1981**, *74*, 5737−5743.
(39) Noodleman, L.; Case, D. A. Density-Functional Theory of Spin Polarization and Spin Coupling in Iron—Sulfur Clusters. *Adv. Inorg. Chem.* **1992**, *38*, 423−458.
(40) Noodleman, L.; Lovell, T.; Han, W.-G.; Liu, T.; Torres, R. A.; Himo, F., In *Comprehensive Coordination Chemistry II, from Biology to Nanotechnology*; Lever, A. B., Ed.; Elsevier Ltd.: New York, 2003; Vol. 2, pp 491−510.
(41) Ciofini, I.; Daul, C. A. DFT Calculations of Molecular Magnetic Properties of Coordination Compounds. *Coord. Chem. Rev.* **2003**, *238-239*, 187−209.
(42) Neese, F. Prediction of Molecular Properties and Molecular Spectroscopy with Density Functional Theory: From Fundamental Theory to Exchange-Coupling. *Coord. Chem. Rev.* **2009**, *253*, 526−563.
(43) Wiig, J. A.; Hu, Y.; Lee, C. C.; Ribbe, M. W. Radical SAM-Dependent Carbon Insertion into the Nitrogenase M-Cluster. *Science* **2012**, *337*, 1672−1675.
(44) Lee, H.-I.; Hales, B. J.; Hoffman, B. M. Metal-Ion Valencies of the FeMo Cofactor in CO-Inhibited and Resting State Nitrogenase by ^{57}Fe Q-Band ENDOR. *J. Am. Chem. Soc.* **1997**, *119*, 11395−11400.
(45) Yoo, S. J.; Angove, H. C.; Papaefthymiou, V.; Burgess, B. K.; Münck, E. Mössbauer Study of the MoFe Protein of Nitrogenase from *Azotobacter Vinelandii* Using Selective ^{57}Fe Enrichment of the M-Centers. *J. Am. Chem. Soc.* **2000**, *122*, 4926−4936.

DOI: 10.1021/acs.jpcc.6b02821
J. Phys. Chem. C XXXX, XXX, XXX−XXX

(46) Harris, T. V.; Szilagyi, R. K. Comparative Assessment of the Composition and Charge State of Nitrogenase FeMo-Cofactor. *Inorg. Chem.* **2011**, *50*, 4811−4824.
(47) Bjornsson, R.; Delgado-Jaime, M. U.; Lima, F. A.; Sippel, D.; Schlesier, J.; Weyhermüller, T.; Einsle, O.; Neese, F.; DeBeer, S. Molybdenum L-Edge XAS Spectra of MoFe Nitrogenase. *Z. Anorg. Allg. Chem.* **2015**, *641*, 65−71.
(48) Bjornsson, R.; Lima, F. A.; Spatzal, T.; Weyhermüller, T.; Glatzel, P.; Bill, E.; Einsle, O.; Neese, F.; DeBeer, S. Identification of a Spin-Coupled Mo(III) in the Nitrogenase Iron-Molybdenum Cofactor. *Chem. Sci.* **2014**, *5*, 3096−3103.
(49) Bjornsson, R.; Neese, F.; Schrock, R. R.; Einsle, O.; DeBeer, S. The Discovery of Mo(III) in FeMoco: Reuniting Enzyme and Model Chemistry. *JBIC, J. Biol. Inorg. Chem.* **2015**, *20*, 447−460.
(50) Spatzal, T.; Schlesier, J.; Burger, E.-M.; Sippel, D.; Zhang, L.; Andrade, S. L. A.; Rees, D. C.; Einsle, O., Nitrogenase FeMoco Investigated by Spatially Resolved Anomalous Dispersion Refinement. *Nat. Commun.* **2016**, *7*.1090210.1038/ncomms10902
(51) Dance, I., A Unified Chemical Mechanism for Hydrogenation Reactions Catalyzed by Nitrogenase. In *Bioinspired Catalysis: Metal-Sulfur Complexes*; Weigand, W., Schollhammer, P., Eds.;Wiley−VCH: Weinheim, 2015.
(52) Hübner, O.; Sauer, J. Structure and Thermochemistry of $Fe_2S_2^{-/0/+}$ Gas Phase Clusters and Their Fragments. B3LYP Calculations. *Phys. Chem. Chem. Phys.* **2002**, *4*, 5234−5243.
(53) Bruska, M. K.; Stiebritz, M. T.; Reiher, M. Analysis of Differences in Oxygen Sensitivity of Fe-S Clusters. *Dalton Trans.* **2013**, *42*, 8729−8735.
(54) Wang, X.-B.; Niu, S.; Yang, X.; Ibrahim, S. K.; Pickett, C. J.; Ichiye, T.; Wang, L.-S. Probing the Intrinsic Electronic Structure of the Cubane [4Fe-4S] Cluster: Nature's Favorite Cluster for Electron Transfer and Storage. *J. Am. Chem. Soc.* **2003**, *125*, 14072−14081.
(55) Niu, S.; Ichiye, T. Cleavage of [4Fe-4S]-Type Clusters: Breaking the Symmetry. *J. Phys. Chem. A* **2009**, *113*, 5710−5717.
(56) Dance, I. Protonation of Bridging Sulfur in Cubanoid Fe_4S_4 Clusters Cause Large Geometric Changes: The Theory of Geometric and Electronic Structure. *Dalton Trans.* **2015**, *44*, 4707−4717.
(57) Esrafili, M. D.; Rezaei, S.; Eftekhari, E. A Theoretical Investigation on Geometry and Electronic Structure of Small Fe_mS_n Nanoclusters ($1 \leq m,n \leq 4$). *Comput. Theor. Chem.* **2012**, *1001*, 1−6.
(58) Yin, S.; Wang, Z.; Bernstein, E. R. Formaldehyde and Methanol Formation from Reactions of Carbon Monoxide and Hydrogen on Neutral Fe_2S_2 Clusters in the Gas Phase. *Phys. Chem. Chem. Phys.* **2013**, *15*, 4699−4706.
(59) Steinfeld, J. I.; Francisco, J. S.; Hase, W. L. *Chemical Kinetics and Dynamics*, 2nd ed.; Prentice Hall: Upper Saddle River, 1999.
(60) Bernhardt, T. M.; Hagen, J.; Lang, S. M.; Popolan, D. M.; Socaciu-Siebert, L. D.; Wöste, L. Binding Energies of O_2 and CO to Small Gold, Silver, and Binary Silver-Gold Cluster Anions from Temperature Dependent Reaction Kinetics Measurements. *J. Phys. Chem. A* **2009**, *113*, 2724−2733.
(61) Liu, T.; Temprano, I.; Jenkins, S. J.; King, D. A.; Driver, S. M. Nitrogen Adsorption and Desorption at Iron Pyrite $FeS_2\{100\}$ Surfaces. *Phys. Chem. Chem. Phys.* **2012**, *14*, 11491−11499.
(62) Sacchi, M.; Galbraith, M. C. E.; Jenkins, S. J. The Interaction of Iron Pyrite with Oxygen, Nitrogen and Nitrogen Oxides: A First-Principles Study. *Phys. Chem. Chem. Phys.* **2012**, *14*, 3627−3633.
(63) Reiher, M.; Hess, B. A. A Quantum-Chemical Study of Dinitrogen Reduction at Mononuclear Iron-Sulfur Complexes with Hints to the Mechanism of Nitrogenase. *Chem. - Eur. J.* **2002**, *8*, 5332−5339.
(64) Machado, F. B. C.; Davidson, E. R. N_2 Activation by Iron-Sulfur Complexes. *Theor. Chim. Acta* **1995**, *92*, 315−326.
(65) Siegbahn, P. E. M.; Westerberg, J.; Svensson, M.; Crabtree, R. H. Nitrogen Fixation by Nitrogenases: A Quantum Chemical Study. *J. Phys. Chem. B* **1998**, *102*, 1615−1623.
(66) Stavrev, K. K.; Zerner, M. C. A Theoretical Model for the Active Site of Nitrogenase. *Chem. - Eur. J.* **1996**, *2*, 83−87.
(67) Rod, T. H.; Hammer, B.; Nørskov, J. K. Nitrogen Adsorption and Hydrogenation on a $MoFe_6S_9$ Complex. *Phys. Rev. Lett.* **1999**, *82*, 4054−4057.
(68) Rod, T. H.; Nørskov, J. K. Modeling the Nitrogenase FeMo Cofactor. *J. Am. Chem. Soc.* **2000**, *122*, 12751−12763.
(69) Hinnemann, B.; Nørskov, J. K. Chemical Activity of the Nitrogenase FeMo Cofactor with a Central Nitrogen Ligand: Density Functional Study. *J. Am. Chem. Soc.* **2004**, *126*, 3920−3927.
(70) Hinnemann, B.; Nørskov, J. K. Structure of the FeFe-Cofactor of the Iron-Only Nitrogenase and Possible Mechanism for Dinitrogen Reduction. *Phys. Chem. Chem. Phys.* **2004**, *6*, 843−853.
(71) Zhong, S.-J.; Liu, C.-W. Possible Binding Modes for Dinitrogen Activation by the FeMo-Cofactor in Nitrogenase. *Polyhedron* **1997**, *16*, 653−661.
(72) Laidler, K. J. *Chemical Kinetics*; Harper Collins: New York, 1987.
(73) Marcus, R. A. Unimolecular Dissociation and Free Radical Recombination Reactions. *J. Chem. Phys.* **1952**, *20*, 359−364.
(74) Dance, I. The Chemical Mechanism of Nitrogenase: Calculated Details of the Intramolecular Mechanism for Hydrogenation of η^2-N_2 on FeMo-co to NH_3. *Dalton Trans.* **2008**, 5977−5991.
(75) Dance, I. The Chemical Mechanism of Nitrogenase: Hydrogen Tunneling and Further Aspects of the Intramolecular Mechanism for Hydrogenation of η^2-N_2 on FeMo-co to NH_3. *Dalton Trans.* **2008**, 5992−5998.
(76) Rod, T. H.; Logadottir, A.; Nørskov, J. K. Ammonia Synthesis at Low Temperatures. *J. Chem. Phys.* **2000**, *112*, 5343−5347.
(77) Lide, D. R. *Handbook of Chemistry and Physics*, 76th ed.; CRC Press: Boca Raton, 1995.

DOI: 10.1021/acs.jpcc.6b02821
J. Phys. Chem. C XXXX, XXX, XXX−XXX